



RESEARCH ARTICLE

10.1002/2016WR019448

Special Section:

Concentration-discharge
Relations in the Critical Zone

Key Points:

- Subsurface conductivity profile, mineral weathering reaction kinetic and flow rate interact together, and influence stream C-Q relation
- An increase in subsurface vertical heterogeneity in K_s can enhance inverse stream C-Q relation for some (but not all) minerals
- Minerals with small ratio of $\frac{C_{eq}}{R_{max}}$ can cause chemostatic C-Q relation regardless of the degree of vertical heterogeneity in K_s

Correspondence to:

A. A. Ameli,
ali.ameli@usask.ca

Citation:

Ameli, A. A., K. Beven, M. Erlandsson, I. F. Creed, J. J. McDonnell and K. Bishop (2017), Primary weathering rates, water transit times, and concentration-discharge relations: A theoretical analysis for the critical zone, *Water Resour. Res.*, 53, 942–960, doi:10.1002/2016WR019448.

Received 1 JUL 2016

Accepted 15 DEC 2016

Accepted article online 27 DEC 2016

Published online 31 JAN 2017

Primary weathering rates, water transit times, and concentration-discharge relations: A theoretical analysis for the critical zone

Ali A. Ameli^{1,2,3} , Keith Beven^{3,4} , Martin Erlandsson⁵, Irena F. Creed² , Jeffrey J. McDonnell^{1,6,7}, and Kevin Bishop^{3,8} 

¹Global Institute for Water Security, University of Saskatchewan, Saskatoon, Saskatchewan, Canada, ²Department of Biology, Western University, London, Ontario, Canada, ³Department of Earth Sciences, Air Water and Landscape Sciences, Uppsala University, Uppsala, Sweden, ⁴Lancaster Environment Centre, Lancaster University, Lancaster, UK, ⁵Department of Physical Geography, Stockholm University, Stockholm, Sweden, ⁶School of Geosciences, University of Aberdeen, Aberdeen, UK, ⁷Department of Forest Engineering, Resources and Management, Oregon State University, Corvallis, Oregon, USA, ⁸Department of Aquatic Sciences and Assessment, Swedish University of Agricultural Sciences, Uppsala, Sweden

Abstract The permeability architecture of the critical zone exerts a major influence on the hydrogeochemistry of the critical zone. Water flow path dynamics drive the spatiotemporal pattern of geochemical evolution and resulting streamflow concentration-discharge (C-Q) relation, but these flow paths are complex and difficult to map quantitatively. Here we couple a new integrated flow and particle tracking transport model with a general reversible Transition State Theory style dissolution rate law to explore theoretically how C-Q relations and concentration in the critical zone respond to decline in saturated hydraulic conductivity (K_s) with soil depth. We do this for a range of flow rates and mineral reaction kinetics. Our results show that for minerals with a high ratio of equilibrium concentration (C_{eq}) to intrinsic weathering rate (R_{max}), vertical heterogeneity in K_s enhances the gradient of weathering-derived solute concentration in the critical zone and strengthens the inverse stream C-Q relation. As $\frac{C_{eq}}{R_{max}}$ decreases, the spatial distribution of concentration in the critical zone becomes more uniform for a wide range of flow rates, and stream C-Q relation approaches chemostatic behavior, regardless of the degree of vertical heterogeneity in K_s . These findings suggest that the transport-controlled mechanisms in the hillslope can lead to chemostatic C-Q relations in the stream while the hillslope surface reaction-controlled mechanisms are associated with an inverse stream C-Q relation. In addition, as $\frac{C_{eq}}{R_{max}}$ decreases, the concentration in the critical zone and stream become less dependent on groundwater age (or transit time).

1. Introduction

The stream concentration-discharge (C-Q) relation is a fundamental description of spatiotemporal feedbacks between hydrological, geochemical, and biological processes in the critical zone [Evans and Davies, 1998; Herndon et al., 2015]. Nevertheless, it subsumes the process complexities of the critical zone into a measure of integrated behavior that can readily be used to identify impacts of climate and land-use changes on ecosystem function [Godsey et al., 2009; Ibarra et al., 2016; Manning et al., 2013]. Given the ease of measuring stream concentration and discharge, it is tempting to infer the interactions among hydrological and geochemical processes such as chemical weathering from the C-Q relation [Anderson et al., 1997; Godsey et al., 2009]. But the variation in chemistry of stream and critical zone water is a function of the different subsurface flow regimes it contains. Linking these flow regimes and their corresponding transit times (the elapsed time that particles spend traveling through subsurface) to the internal weathering regime in the critical zone and ultimately integrated catchment-scale C-Q pattern (and unpacking such relations) is a grand challenge for critical zone science.

Evans and Davies [1998] and Chanut et al. [2002] suggested that the form and direction of the hysteresis loop of the stream C-Q relation can aid in estimation of the relative contribution of sources of stream solutes under different flow regimes and antecedent moisture conditions. Flow rate influences mixing, source,

production, and mobilization rate of weathering-derived solutes by altering flow pathlines through soil horizons [Bishop *et al.*, 2004; Herndon *et al.*, 2015]. For example, Anderson *et al.* [1997] and Anderson and Dietrich [2001] used detailed measurements of soil water, bedrock water, and stream concentrations during natural and artificial precipitation events to show that the relative bedrock and soil contributions to stream concentration of weathering products (i.e., base cations, silica, and alkalinity) varied with stream discharge. They also showed that both soil and bedrock concentrations were affected by subsurface flow rate; they become more dilute at high flow and more concentrated at low flow. Neal *et al.* [1992], McGlynn and McDonnell [2003], and many others have similarly attributed stream chemistry variations to changes in dominant water inputs to the stream, from deeper groundwater during base flow to shallower hillslope runoff (e.g., subsurface storm flow [Ameli *et al.*, 2015] and transmissivity feedback [Bishop *et al.*, 2011]) at high flow.

Another factor affecting the relation between primary weathering rates and stream C-Q is groundwater transit time (or age) which reveals the contact time of water with mineral surfaces in the subsurface. Burns *et al.* [1998, 2003] used hillslope-scale measurements of concentration and groundwater age at the Panola Mountain Research Watershed to show that the concentration of weathering products was positively correlated to groundwater age. More recently, Maher [2010, 2011] used a reactive transport model to suggest that weathering rates within the critical zone depend strongly on fluid transit time. The age dependency of the subsurface weathering could justify the widespread observation that stream concentrations of weathering products can decrease with increasing stream discharge (i.e., inverse C-Q relations as shown in, e.g., Clow and Drever [1996], Hem [1948], and Johnson *et al.* [1969]). This could be attributed to the fact that faster waters with shorter transit times and therefore shorter contact time with minerals are discharged into the stream with a lower concentration of weathering products [e.g., Anderson *et al.*, 1997; Pilgrim *et al.*, 1979].

While flow path and age provide fundamental insights into the integrated stream C-Q relation, many environments show only slight change in streamflow concentration even when stream discharge (and therefore, presumably, subsurface transit times and pathways) vary considerably. This chemostatic behavior was described by Godsey *et al.* [2009] who showed for 59 watersheds in the USA that streams draining volcanic bedrock had steeper clockwise inverse C-Q relations than sites with carbonate bedrock that showed significantly shallower C-Q relations. This was surprising as discharge and mean subsurface transit time (MTT) varied by several orders of magnitude spatially and temporally within each watershed and between watersheds [Godsey *et al.*, 2009]. Similar chemostatic C-Q behavior has been seen in granitic boreal catchments in permafrost regions of Russia [Zakharova *et al.*, 2005] and many other environments [Ibarra *et al.*, 2016; Moon *et al.*, 2014; Torres *et al.*, 2015].

So what is the way forward for understanding the links between primary weathering rates, subsurface flow pathways, transit times, and stream C-Q relations? Perhaps the simplest conceptualization of the solute flux composition of stream water is that this flux is the average of the solute composition along different shallow and deep flow pathlines discharged into the stream [Maher and Druhan, 2014]. The wide range of transit times along these flow pathlines comprises the catchment transit time distribution (TTD). The TTD thus contains information about the variation of contact time between water particles and mineral surfaces along different pathlines. The subsurface flow pathline distribution, together with the TTD, is themselves a complex measure of subsurface macroheterogeneity and microheterogeneity [Ameli *et al.*, 2016a, 2016b; Davies and Beven, 2015; Kirchner, 2016a] that influence weathering regimes in the critical zone as well as the stream C-Q relation [Anderson *et al.*, 1997; Herndon *et al.*, 2015].

But the “weathering” that the TTD and subsurface flow pathlines may influence is an exquisitely complex set of processes in its own right. To begin with, different minerals react at different rates toward different equilibrium concentrations with a given set of conditions (e.g., pH, redox, temperature, and solute concentrations). In addition to weathering kinetics, reactive surface area can dramatically vary with depth with less surface area in shallower weathered zones compared to deeper unweathered rock [White *et al.*, 2008, 2009]. Furthermore, the products of primary weathering can then form secondary minerals that have their own set of reactions [Zhu, 2005].

The aforementioned processes take place in a flow system traversing landscapes at velocities that vary in time and space as governed by the structure of the pore space in response to driving forces such as precipitation and evapotranspiration. Weathering rates of some minerals (e.g., carbonate) may be fast enough that the time to equilibrium with the fluid is much shorter than the transit time of water particles in some or all

of the landscape, such that some or all of the fluid is effectively near equilibrium. On the other hand, some silicate minerals have much slower weathering rates, with a time to chemical equilibrium that can be longer than the mean transit time [Godsey *et al.*, 2009]. Given the complexities of how weathering within the landscape is expressed in the stream C-Q relation, we need to explore “specific hypotheses” of how subsurface hydrology interacts with minerals to influence chemical evolution within the critical zone and the resulting patterns of solute concentration in stream runoff. But as yet, our field measurement technology does not often allow us to test such hypotheses directly.

Here we use a 2-D subsurface-stream flow and transport model to explore theoretically how subsurface flow rate, flow pathline, and transit times control the weathering rate of the primary mineral in the critical zone and ultimately the stream concentration of weathering products. Our work builds on the hydrological model developed in Ameli *et al.* [2016a] and tested in Ameli *et al.* [2016b], where we integrated saturated-unsaturated flow and particle tracking transport models in hillslopes with exponential vertical decline in saturated hydraulic conductivity (K_s). This permeability pattern is typical in forested till catchments, where the distribution of weathering and the transfer of weathering products to the stream may be strongly influenced by how flow pathline dynamics are influenced by the characteristic architecture of soil permeability. Soil permeability can decline rapidly with depth, forcing much of the lateral flow closer to the soil surface. Our physically based model is able to explicitly track particles and determine their concentrations, pathlines, and transit time distributions in the critical zone and stream as well as the young water fraction in streamflow (as defined recently by Kirchner [2016a] and Jasechko *et al.* [2016]) under steady state assumptions. We now link the model with a general reversible Transition State Theory style (TST-style) weathering dissolution rate law to explore how the subsurface conductivity profile (represented here by vertical exponential decline in K_s), water flow rates, pathlines, transit times, and primary mineral weathering properties (e.g., intrinsic weathering rate and weathering equilibrium concentration) interact to generate distinct weathering regimes in the critical zone and ultimately different C-Q-relations in the stream. The weathering regime is characterized using the Damköhler number (defined as the ratio between mean transit time and time to chemical equilibrium [e.g., Johnson and DePaolo, 1994; Lebedeva *et al.*, 2007]) to determine the shift between transport-control and surface reaction-control on weathering in the critical zone.

It is important to note that the simple particle tracking based hydrogeochemical approach used here cannot be considered a full geochemical treatment [cf. Atchley *et al.*, 2014] that takes into account factors such as the impact of reactive surface area and the vertical mineral gradients that develop over time. Instead, our work advances understanding of the controls created by the primary weathering of minerals as one component of the complete “picture.” Our work responds to calls made by McDonnell and Beven [2014] for a model that differentiates flow velocities, celerities, and transit times. Most importantly, our work responds to calls made by Godsey *et al.* [2009] and Maher and Druhan [2014] for an internally consistent model of hydrology, chemical weathering, and transport, with the ability to consider geomorphic features including soil depth and saturated hydraulic conductivity patterns, pathlines, and transit times in both saturated and unsaturated domains, as well as mineral reaction kinetics to explore controls on chemical evolution in the critical zone.

We ask the following questions:

1. How does the subsurface conductivity profile interact with different mineral reaction (and solubility) kinetics to influence the hillslope-scale distribution of weathering-derived solute concentrations, time to chemical equilibrium, and the Damköhler number?
2. How do different weathering regimes in the critical zone (i.e., transport-controlled versus surface reaction-controlled) lead to different stream C-Q relations?
3. What are the combinations of mineral reaction kinetics and subsurface conductivity profiles that result in inverse and chemostatic C-Q relations in streams?
4. To what extent do stream C-Q relations and hillslope concentration depend on particle transit times?

2. Methods

We extended the integrated steady state flow and random walk particle tracking model developed in Ameli *et al.* [2016a] (briefly explained here in section 2.1 and Appendix A) to take into account chemical evolution

along subsurface flow pathlines (section 2.2). The hydrological and geochemical properties of the hypothetical hillslope used in our theoretical experiment are also explained in section 2.3.

2.1. Flow and Particle Tracking Transport Model

The mathematical formulation used in the model to calculate the maps of hydraulic head and velocity in both saturated and unsaturated zones are explained in Appendix A. Once the maps of velocity are calculated, the following equation is used to describe the step of a water particle (p) in the random walk particle tracking method:

$$\text{in the unsaturated zone : } x_p^k = x_p^{k-1} + (V_{uxr})_p^k \Delta t \ \& \ z_p^k = z_p^{k-1} + (V_{uzr})_p^k \Delta t \quad (1a)$$

$$\text{in the saturated zone : } x_p^k = x_p^{k-1} + (V_{sxr})_p^k \Delta t \ \& \ z_p^k = z_p^{k-1} + (V_{szz})_p^k \Delta t \quad (1b)$$

where x_p^k and z_p^k are the position of the particle (p) at the k th time step. For each particle (p) and each time step (k), V_{uxr} and V_{uzr} denote random numbers drawn from an exponential distribution with a mean of V_{ux} and V_{uz} , respectively. V_{ux} and V_{uz} (equation (A5)) are unsaturated zone mean pore water velocities in x and z directions for each particle at each time step. These are calculated throughout the unsaturated hillslope using the semianalytical physically based approach (Appendix A). Similarly, V_{sxr} and V_{szz} denote random numbers drawn from an exponential distribution with a mean of V_{sx} and V_{sz} , respectively; where V_{sx} and V_{sz} (equation (A6)) are saturated zone mean pore water velocities in x and z directions at each particle and each time step. A small value of time difference between time steps ($\Delta t = 0.001$ d) was assumed for all examples solved in this paper to ensure precise calculation of particles locations and their concentration evolution.

It is important to note that the application of an exponential distribution in the random walk particle tracking approach, rather than the commonly used Gaussian distribution, aims to provide for a higher probability of a particle being in a relatively slow pathway as well as some local preferential flow [see also *Davies et al., 2011; Davies et al., 2013*]. Velocities are assumed to be independent between time steps, which means that

the integral or Lagrangian velocities over longer pathlines will tend toward a Gaussian distribution. All particles were initially released at evenly spaced locations (with an increment of 25 cm at a total of 560 locations) along the topographic surface and ultimately discharged into the stream as schematically shown in Figure 1. The transit time of each water particle is the time that the particle spends traveling through the subsurface from when it is released along the topographic surface to when it discharges into the stream. For a given steady state discharge (Q), time-invariant transit time distribution (TTD), and mean transit time (MTT) are thus the probability density function and average of transit times of all 560 water particles discharged into the stream, respectively.

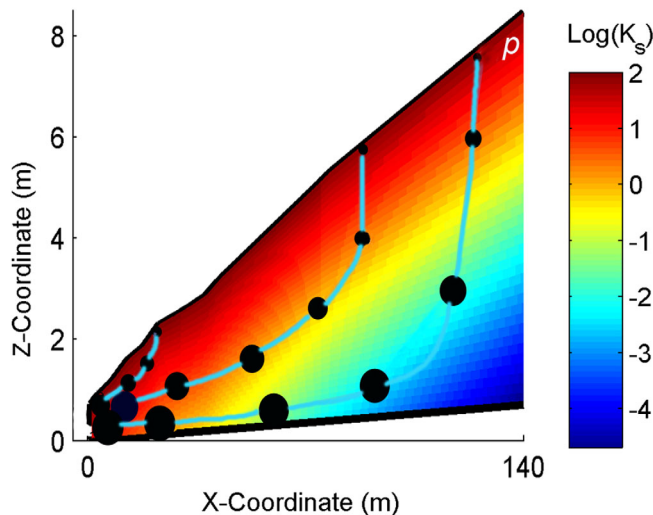


Figure 1. Hypothetical hillslope geometry of exponential decline in saturated hydraulic conductivity (K_s , (m/d)) with depth (color map shows the K_s pattern). The stream is located at $x = 0$ (white gap). The value of α (the parameter of the exponential relationship between K_s with soil depth) was assumed as 2 (1/m) and K_{s0} (the saturated hydraulic conductivity along the topographic surface) was assumed as 100 m/d in this example. This figure also shows the conceptual schematic of chemical flow evaluation along three hypothetical flow pathlines in the hillslope. In this conceptualization, each particle (p) enters the hillslope with a known initial concentration (C_p^0) of weathering-derived products (small circle). The concentration of weathering products of each particle along its flow pathline increases (particle becomes larger in this schematic) until the equilibrium concentration (C_{eq}) with the mineral is reached (the largest circle). In this conceptual schematic, only particles that traverse deep low-permeable (and potentially unweathered) rock reaches equilibrium before it enters the stream.

2.2. Concentration Evolution Along the Flow Pathlines

To calculate the concentration of weathering products along flow pathlines using a particle tracking method, we applied the widely used approximation that the concentration of

weathering products along the flow pathlines increase until the equilibrium concentration (at a given set of temperature and pH) with the mineral is reached [Drever, 1988; Maher and Chamberlain, 2014]. A similar particle tracking algorithm has been recently coupled to numerical flow models (e.g., ParFlow) to explore reactive transport in groundwater systems [e.g., Atchley et al., 2014; Cui et al., 2014; Siirila and Maxwell, 2012]. Of course this mechanism is only one of many processes affecting chemical evolution along the flow pathlines, which include ionic exchange, complexation with DOC and reactive gases, as well as precipitation of secondary phases [Brantley et al., 2011; Drever, 1994; Gaillardet et al., 2011; Oliva et al., 1999]. The evolution of chemical weathering concentration (C) for each particle p and at each time step k (i.e., C_p^k) can be calculated as

$$C_p^k = C_p^0 + R(C_p^{k-1}) \Delta t \quad (2)$$

where $R(C)$ refers to the dissolution rate and C_p^0 is the initial concentration at the land surface. An identical initial concentration of 10^{-8} (mol/L) was assumed for the all particles in examples solved in this paper. R is determined through Transition State Theory style dissolution rate law as discussed in section 2.3.2. Figure 1 schematically shows that how the concentration of each particle increases as it moves toward the stream; albeit the rate of the increase varies depending upon the particle pathways and locations as well as concentration. The stream concentration (C_R), for a given steady state flow rate (Q), is the average concentrations of all 560 particles discharged into the stream. The time and length that 560 particles spend on average to reach chemical equilibrium (i.e., particle concentration becomes equal to equilibrium concentration— C_{eq}) before being discharged into the stream is also calculated to estimate the time to equilibrium (T_{eq}) and length to equilibrium (L_{eq}) for each example; albeit only particles reaching chemical equilibrium before being discharged are considered in this calculation.

2.3. Hillslope Hypothetical Properties

Figure 1 depicts the general schematic of a shallow 2-D hillslope located in the vicinity of a water course (i.e., stream), used here to perform theoretical experiments on how subsurface hydrology interacts with mineral reaction kinetics and influences chemical weathering in the critical zone to ultimately yield stream C-Q relations.

2.3.1. Hillslope Description and Hydrological Properties

Two hypothetical patterns of exponential decline in K_s with soil depth were assumed— $\alpha = 2$ [1/m] (Figure 1) and $\alpha = 0$, where α refers to the parameter of the exponential relationship between K_s with soil depth. The former case refers to a heterogeneous hillslope of rapidly declining K_s with depth and the latter case refers to a homogeneous hillslope. The average K_s throughout the hillslope was held constant in both cases to facilitate a focus on the influence of the rate of exponential decline in K_s with depth. Thus, while a K_{s0} (saturated hydraulic conductivity along the topographic surface) of 100 m/d was assumed for the heterogeneous case with $\alpha = 2$ (Figure 1), a uniform K_s of 20 m/d (average K_s of the former case throughout the hillslope) was considered throughout the hillslope for the homogeneous case with $\alpha = 0$. A porosity-depth relationship of $\theta_s(x, z) = 0.49e^{0.26(z-Z_t)}$ was also assumed for both cases. Gardner [1958] unsaturated parameters characterizing the hydraulic conductivity in the unsaturated zones were also assumed as $\beta = 1$ (1/m) and $\varphi^e = 0.05$ m (equation (A1)). Five discharge (Q) rates of 0.2, 0.5, 0.8, 1, and 2 mm/d were also considered for our theoretical experiments. The assumed geometry of the hillslope, discharge rates, and material properties are consistent with the properties of the widely studied S-Transect hillslope within the Krycklan till-mantled watershed in the boreal zone of Sweden's forest landscape where till-mantled watersheds have K_s values that can be hypothesized to decay exponentially with depth at an exponential rate of up to $\alpha = 4$ (1/m) [Ameli et al., 2016b; Bishop et al., 2011]. The assumed steady state discharge rates also span the range between the 10th percentile (0.2 mm/d) and 90th percentile (2 mm/d) observed daily discharge at the S-Transect during the 30 year period from 1980 to 2010.

2.3.2. Geochemical Properties

The mineral dissolution rate depends on several factors, where pH and temperature are generally thought to be the most important as they can cause dissolution rates to vary by several orders of magnitudes [Hellmann, 1994; Sverdrup, 1990]. Concentrations of aluminum [Oelkers et al., 1994], base cations [Oelkers and Schott, 2001], organic acids [Drever and Stillings, 1997], and carbon dioxide pressure [Golubev et al., 2005] have also been shown to affect dissolution rates. However, most mineral dissolution experiments have been conducted at far-from-equilibrium conditions, and often at extreme pH-values and high temperatures. Mineral dissolution at field conditions is considerably slower and the behavior near equilibrium is uncertain.

In chemical weathering models, the Transition State Theory style (TST-style) relationship [Eyring, 1935] is often employed to describe mineral dissolution characteristics from far- to very close-to-equilibrium [God-d ris et al., 2006; Lasaga, 2014; Lasaga and Kirkpatrick, 1981; Maher et al., 2009; Oelkers et al., 1994; Palandri and Kharaka, 2004]. This approach suggests that far from equilibrium (where the concentration is close to zero) the mineral dissolution rate is almost unaffected by the aqueous concentration, but ultimately decreases abruptly when the fluid concentration of the weathering product approaches the close vicinity of the equilibrium concentration. This could also of course vary in different parts of the pore space structure (and thus leads to local concentration gradients), but such differences are necessarily assumed negligible here. The general reversible form of the TST-style relationship between dissolution rate and saturation state can then be given by

$$R(c) = R_{max} \left(1 - \frac{C}{C_{eq}} \right)^b \tag{3}$$

where R_{max} is the maximum or intrinsic (laboratory) dissolution rate, C_{eq} refers to the equilibrium concentration of fluid in contact with the mineral, and b is a constant that determines the shape of the TST-style relationship as well as the concentration at which the dissolution rate decreases abruptly.

Here we considered five hypothetical minerals through the implementation of different R_{max} and C_{eq} values in TST-style relationships with an identical b equal to 0.1 (Figure 2). Intrinsic weathering rate (R_{max}) of minerals increases among M_1 , M_b , and M_2 with an identical equilibrium concentration (C_{eq}); thus the ratio of $\frac{C_{eq}}{R_{max}}$, which is known as the mineral theoretical time to equilibrium, decreases. On the other hand, C_{eq} decreases among M_3 , M_b , and M_4 with an identical R_{max} and thus the ratio of $\frac{C_{eq}}{R_{max}}$ decreases. The $\frac{C_{eq}}{R_{max}}$ of the selected hypothetical minerals with a range from 357 day to 14 day can span the weathering kinetics of the minerals used in other studies such as $\frac{C_{eq}}{R_{max}} \approx 146$ d in Maher and Druhan [2014] and $\frac{C_{eq}}{R_{max}} \approx 74$ d in Maher [2011]. Furthermore, these hypothetical mineral weathering characteristics can span approximately realistic geochemical behavior for a wide range of silicate and phosphate minerals under various pH and temperature conditions at the S-Transect hillslope [Erlandsson et al., 2016]. For example, within the S-Transect hillslope, C_{eq} can vary between 1×10^{-6} (mol/L) (which is the K-concentration of where K-feldspar reaches equilibrium) and 1×10^{-4} (mol/L) (which is the Ca-concentration at 10 m depth where some minerals are close to saturated conditions). Note that these two elements (Ca and K) define the range for major weathering products at the hillslope. In the same hillslope, the largest flux from a single mineral was reported as 1.4×10^{-7} (mol/L/d) which is the calculated (modeled) flux of base cation release through plagioclase dissolution.

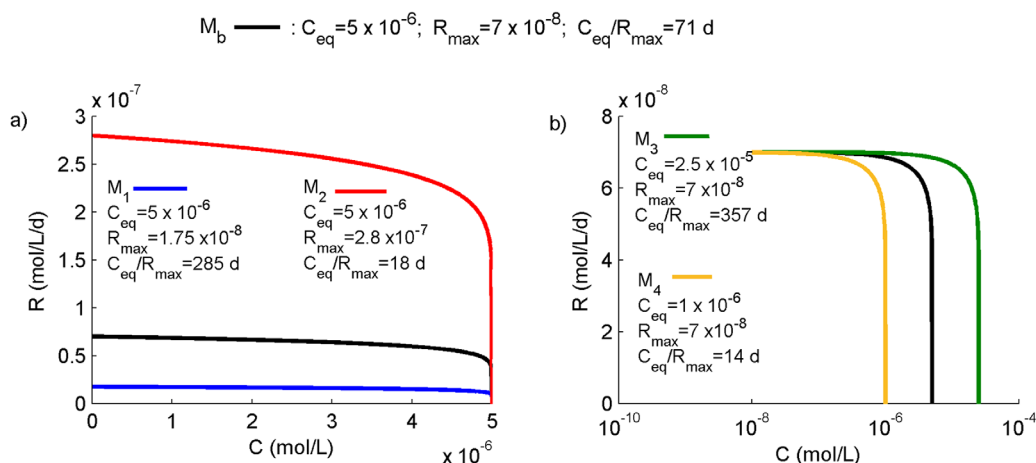


Figure 2. General reversible Transition State Theory style (TST-style) function used to characterize the relation between dissolution rate (R) and concentration (C) for five theoretical minerals (M_b , M_1 , M_2 , M_3 , M_4). (a) Minerals M_b , M_1 , and M_2 with identical C_{eq} but different R_{max} . (b) Minerals M_b , M_3 , and M_4 with identical R_{max} but different C_{eq} . The ratio of $\frac{C_{eq}}{R_{max}}$ is known as the mineral theoretical time to equilibrium which decreases among M_1 , M_b , and M_2 as well as among M_3 , M_b , and M_4 .

3. Results

3.1. Subsurface Flow Pathline and Transit Time Distribution

As α (the parameter of exponential decline in k_s with depth) increases, deep and shallow subsurface pathlines lessen and increase, respectively, for the wide range of subsurface flow rates considered here (Figure 3). The proportion of fast-arrival waters discharged into the stream also increases as α increases (Figure 3—inset). Furthermore, the simulated ratio of unsaturated zone mean transit time to saturated zone mean transit time ($\tau_{u/s}$) decreases. These findings can be attributed to the fact that the water table (green lines in Figure 3) rises nearer to the ground surface where saturated hydraulic conductivity is relatively higher for the case with $\alpha = 2$ (and $K_{s0} = 100$ m/d) than the more homogeneous subsurface with $\alpha = 0$ (and $K_{s0} = 20$ m/d). This rise in the water table (and thus decline in the unsaturated zone thickness) can also be inferred from the decrease in average depth to water table (parameter d in Figure 3).

3.2. Stream Concentration-Discharge Relation

Stream concentrations for five hypothetical minerals (M_b, M_1, M_2, M_3, M_4) and two different exponential rates ($\alpha = 2$ and $\alpha = 0$) of exponential decline in K_s with soil depth are calculated for a range of flow rates. The mineral's ratio of $\frac{C_{eq}}{R_{max}}$ decreases among M_1, M_b , and M_2 as well as among M_3, M_b , and M_4 ; among the former group of minerals C_{eq} is constant but R_{max} increases, and for the latter group of minerals C_{eq} decreases but R_{max} is constant (Figure 2). The concentrations discharged into the stream are also subdivided

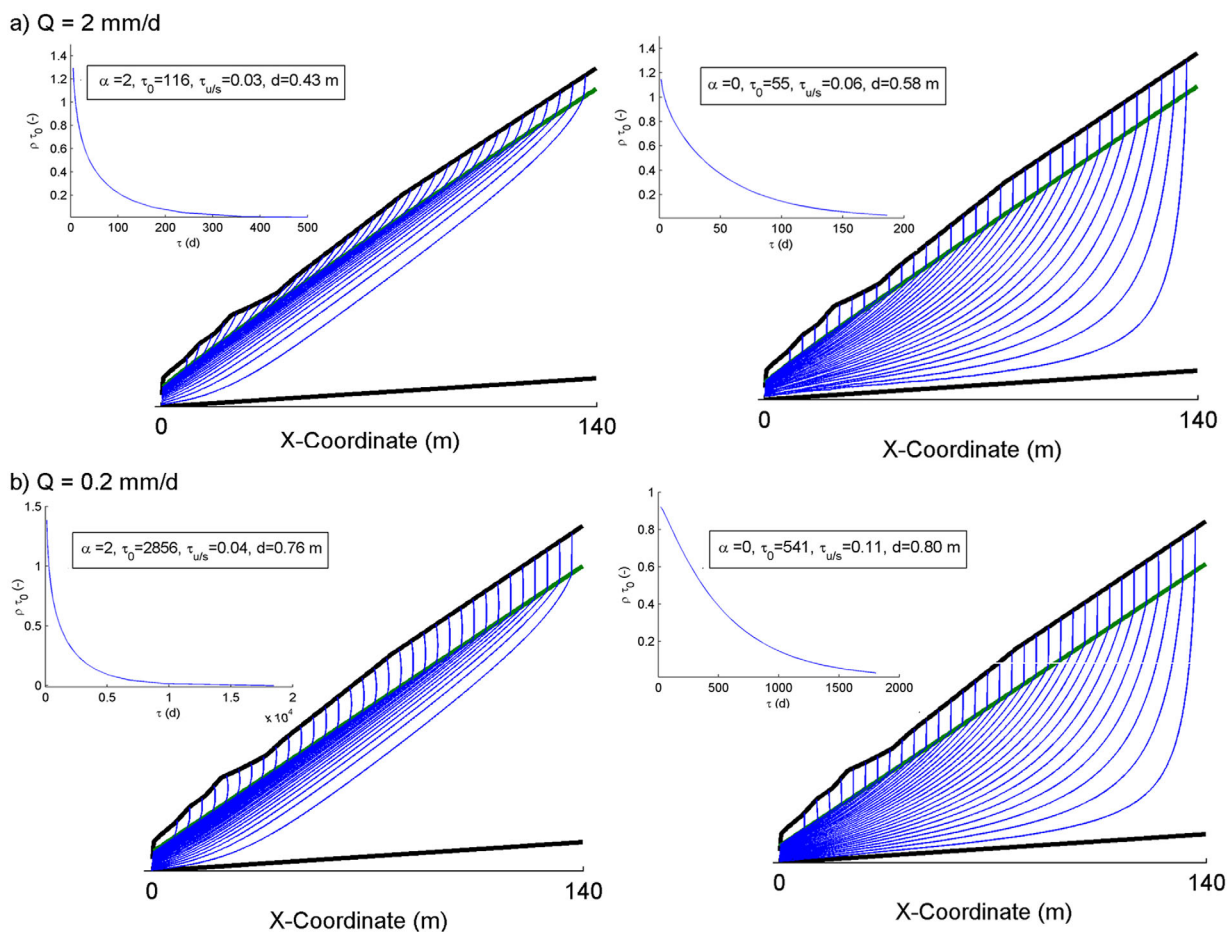


Figure 3. Subsurface flow pathlines (blue lines), water table location (green line), and Transit Time Distribution (ρ -probability density function of transit times as shown in inset) for two hypothetical rates of exponential decline in saturated hydraulic conductivity, one where $\alpha = 2$ (left) and the other where $\alpha = 0$ (right). Of the five streamflow (discharge) rates considered in this paper, only two are shown here (maximum and minimum rates) for both values of α : (a) $Q = 2$ mm/d; and (b) $Q = 0.2$ mm/d. τ_0 (day) represents mean transit time and $\tau_{u/s}$ refers to the ratio between mean transit time in the unsaturated zone and the saturated zone. Probability density function (ρ) corresponding to small transit times (τ) depicts the proportion of fast-arrival waters discharged into the stream. Parameter “ d ” refers to the average depth to the water table (or average unsaturated zone thickness). Only $\frac{1}{8}$ of all flow pathlines were shown.

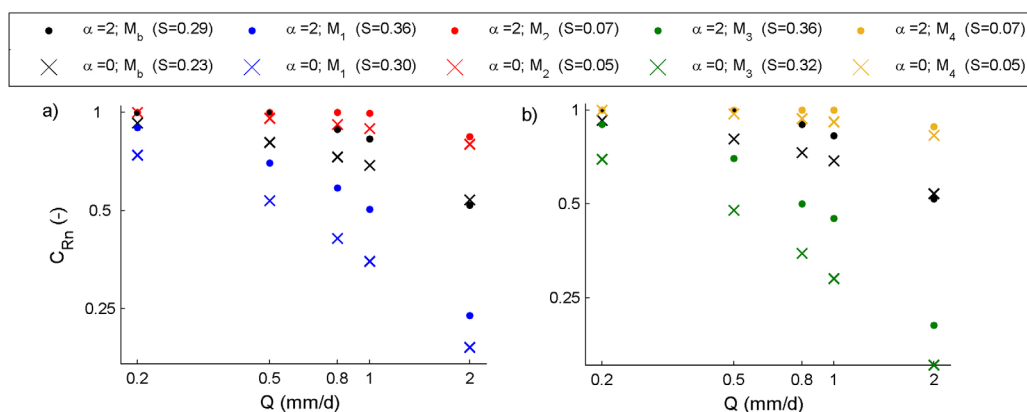


Figure 4. Simulated stream concentration-discharge relation (concentration is normalized with respect to the mineral C_{eq} , log-log scale) for two different exponential rates (α) of exponential decline in saturated hydraulic conductivity with soil depth and for five theoretical minerals. Stream normalized C_{Rn} - Q relation for (a) minerals M_1 , M_b , and M_2 where the mineral's $\frac{C_{eq}}{R_{max}}$ decreases among M_1 , M_b , and M_2 and (b) minerals M_3 , M_b , and M_4 where mineral's $\frac{C_{eq}}{R_{max}}$ decreases among M_3 , M_b , and M_4 . The parameter S (values in the parenthesis) refers to the slope of the best fit inverse clockwise power-law line (linear in Log-Log scale) to C_{Rn} - Q relation.

into two classes: (1) concentration of young waters (C_{RY}) that is the average concentration of particles with an age <3 months and (2) concentration of old water (C_{OY}) that is the average concentration of particles with an age >3 months. The 3 months age threshold to distinguish young water from old water was recently introduced by Kirchner [2016a]. Stream total concentration (C_R) is the average concentration of all 560 particles discharged into the stream at a given steady state flow rate. For the sake of simplicity of comparison, all types of stream concentrations are normalized (subscript (n)) with respect to the equilibrium concentration of each mineral (Figure 4).

A more heterogeneous subsurface with a larger parameter (α) of vertical exponential decline in K_s enhances the inverse relation between normalized stream concentration (C_{Rn}) and discharge (Q) (Figure 4). Note that the slope (S) of best fit inverse clockwise power-law line to C_{Rn} - Q relation reveals the level of inverse relation between stream concentration and discharge. In addition, the inverse C_{Rn} - Q relation becomes stronger (S becomes larger) as the regolith's $\frac{C_{eq}}{R_{max}}$ increases, regardless of whether R_{max} decreases (among M_2 , M_b , M_1 minerals in Figure 4a) or C_{eq} increases (among M_4 , M_b , M_3 minerals in Figure 4b). Note that results clearly show that C_{Rn} - Q relation cannot exactly embrace a power-law shape (i.e., linear relation in Log-Log scale). This is consistent with the assumption of the model used here that stream concentration cannot exceed equilibrium concentration (C_{eq}) for a range of streamflows including stream low flow.

On the other hand, a decrease in regolith's $\frac{C_{eq}}{R_{max}}$ results in a larger likelihood of chemostatic behavior regardless of the degree of heterogeneity in the vertical pattern of K_s . For example, for the minerals with the lowest $\frac{C_{eq}}{R_{max}}$ (i.e., M_2 and M_4), the stream concentration only slightly declines as stream discharge changes from low flow to high flow conditions with an almost chemostatic C_{Rn} - Q relation (s) for both homogeneous and heterogeneous hillslopes.

The concentrations in the younger (C_{RY}) and older (C_{RO}) components of stream discharge suggest that for all five minerals the concentration in young water declines relative to the concentration in old water as flow rate increases, with a more pronounced (nonlinear) decline in the heterogeneous subsurface with $\alpha = 2$ compared to the homogeneous one with $\alpha = 0$ (Figures 5a and 5b). Although for the low flow, the proportion of stream young water to old water concentration ($\frac{C_{RY}}{C_{RO}}$) in the heterogeneous domain is larger compared to the homogeneous domain, as flow rate increases, $\frac{C_{RY}}{C_{RO}}$ in the heterogeneous domain approaches the homogeneous one. This finding can be attributed to a larger difference between $\tau_{u/s}$ (ratio of unsaturated zone to saturated zone mean transit time) in heterogeneous and homogeneous domains for low flow conditions (Figure 3b) compared to the difference between $\tau_{u/s}$ in heterogeneous and homogeneous domains for high flow conditions (Figure 3a). In addition, Figures 5a and 5b show that as the regolith's $\frac{C_{eq}}{R_{max}}$ decreases (e.g., from M_1 to M_2 and from M_3 to M_4), the concentrations in the younger stream component (C_{RY}) approaches the concentration of the older stream component (C_{RO}).

The relation between normalized stream concentration C_{Rn} and MTT (corresponding to the five flow discharge rates considered here) is also explored (Figures 5c and 5d). As the mineral R_{max} increases or C_{eq}

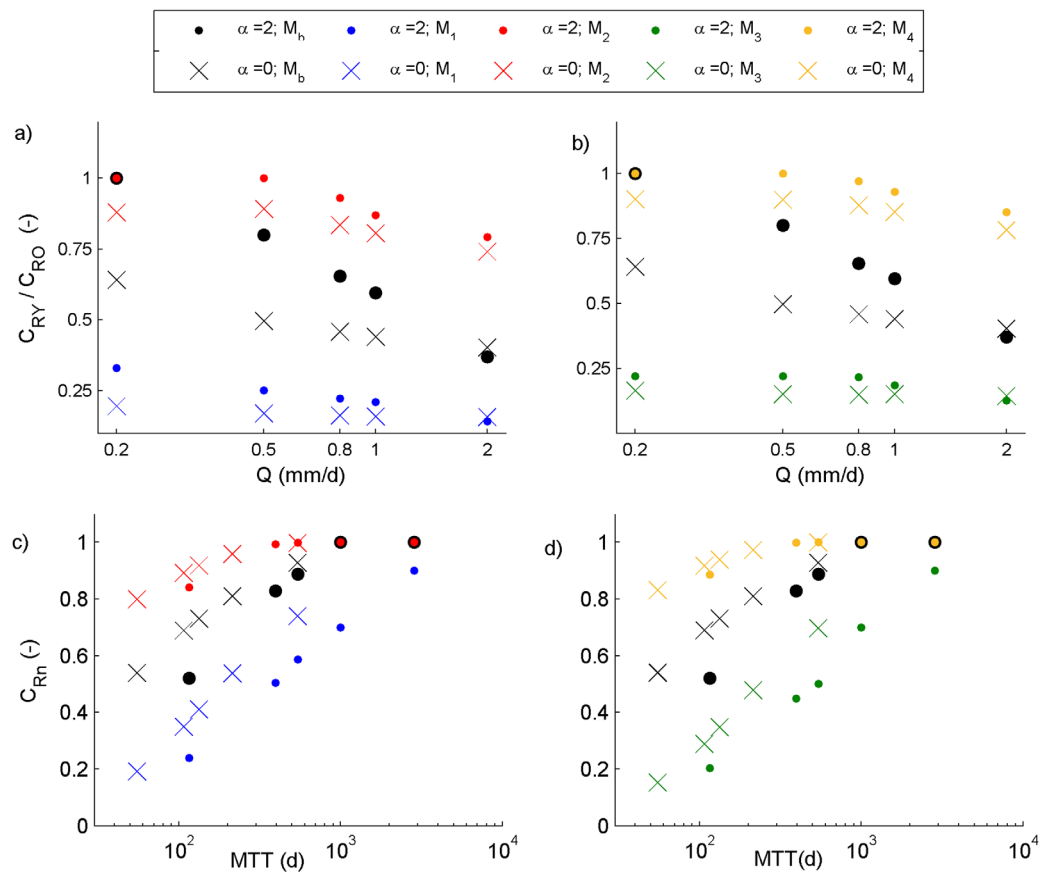


Figure 5. Relation between stream concentration and age of water for different exponential rates (α) of exponential decline in saturated hydraulic conductivity with soil depth, five theoretical minerals (M_b, M_1, M_2, M_3, M_4) and five steady state discharges (as well as their corresponding mean transit time-MTT). The proportion of average concentration of particles with ages <3 months (C_{RY}) relative to average concentration of particles with ages >3 months (C_{RO}) discharged into the stream for (a) minerals M_1, M_b , and M_2 where intrinsic weathering rate (R_{max}) of minerals increases among M_1, M_b , and M_2 with an identical equilibrium concentration (C_{eq}), and (b) minerals M_3, M_b , and M_4 where C_{eq} of minerals decreases among M_3, M_b , and M_4 with an identical R_{max} . Relation between stream normalized concentration (C_{Rn}) and hillslope MTT for (c) minerals M_1, M_b , and M_2 , and (d) minerals M_3, M_b , and M_4 . The regolith's $\frac{C_{eq}}{R_{max}}$ decreases among M_1, M_b , and M_2 as well as among M_3, M_b , and M_4 .

decreases (or in general $\frac{C_{eq}}{R_{max}}$ decreases), the widely accepted positive correlation between hillslope MTT and stream concentration of weathering products is weakened because the concentration along a flow pathline approaches the equilibrium concentration faster. Once equilibrium is reached, more time in the catchment will not generate greater concentrations. In addition, almost similar values of stream concentration can be obtained while hillslope conductivity profile and MTT changes considerably. For example, for the M_b mineral (black dot and black cross), an almost identical normalized stream concentration of 0.52 occurred between homogeneous and heterogeneous K_s patterns, while MTT was 55 days within the former and 116 days within the latter domains (Q was equal to 2 mm/d for both cases).

3.3. Hillslope Internal Weathering Characteristics

3.3.1 Spatial Characteristic of Weathering

The spatial distribution of concentration of weathering products throughout the hillslope depends upon the subsurface conductivity profile as well as the mineral reaction kinetics and solubility (Figure 6). A smaller mineral $\frac{C_{eq}}{R_{max}}$ results in equilibrium being reached closer to the land surface. This is clear for mineral M_2 which has a larger R_{max} compared to M_1 and mineral M_4 which has a smaller C_{eq} compared to M_3 . In addition, concentration gradients throughout the hillslope can be significantly enhanced by rapid exponential decline in K_s (larger α). This is more pronounced for the mineral with the largest $\frac{C_{eq}}{R_{max}}$ (M_1 and M_3). For minerals M_1 and M_3 and within the hillslope with a homogeneous K_s pattern (Figure 6b), no part of the hillslope reaches equilibrium condition at high flow ($Q = 2$ mm/d). Note that the spatial distribution of different minerals

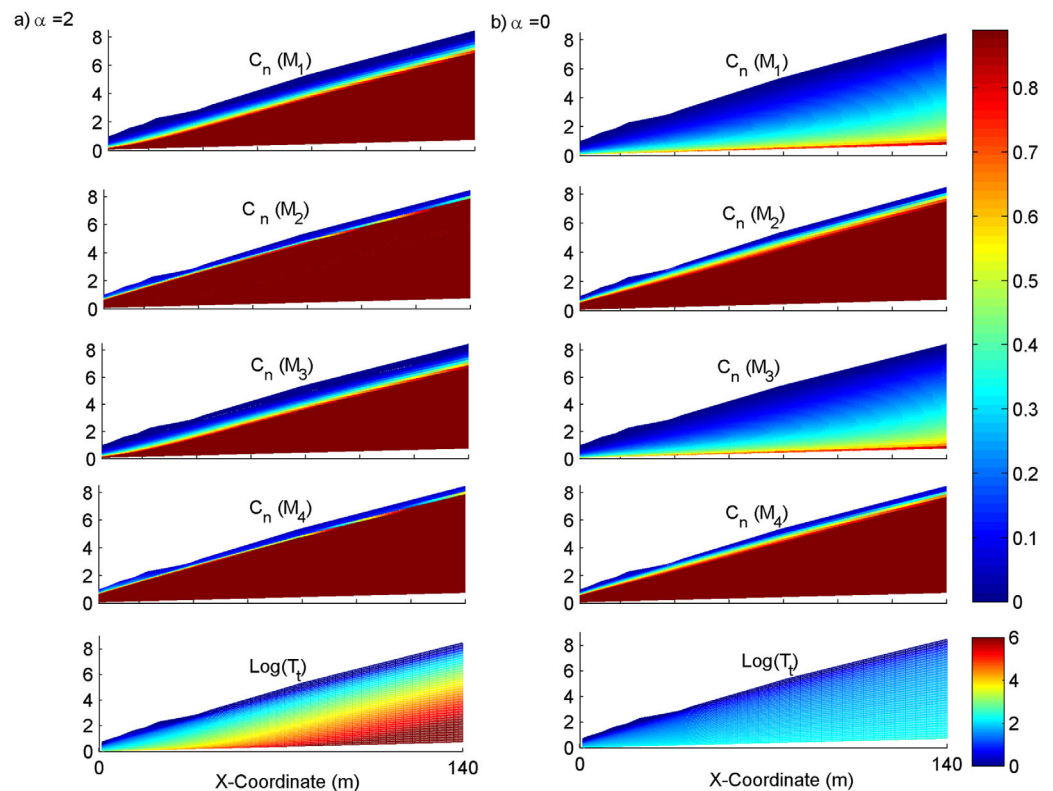


Figure 6. Spatial distribution of fluid concentration (C_n) (normalized with respect to the mineral C_{eq}) for four minerals (M_1, M_2, M_3, M_4) in response to high flow conditions, and the spatial distribution of particle residence times throughout the hillslope (T_r) in response to high flow conditions (last row). Residence time is the time which elapses between when a particle enters the soil at the land surface and when it reaches a given point within the hillslope. (a) Heterogeneous saturated hydraulic conductivity vertical pattern ($\alpha = 2$). (b) Homogeneous saturated hydraulic conductivity pattern ($\alpha = 0$). Only minerals with the two extreme weathering characteristics with regard to R_{max} (M_1, M_2) and C_{eq} (M_3, M_4) are shown (i.e., largest and smallest $\frac{C_{eq}}{R_{max}}$). The behavior of mineral M_0 falls between these pairs of extremes.

with different weathering characteristics within the hillslope could also impact the spatial distribution of weathering, but assessment of this factor is beyond the scope of this paper.

In addition, mineral reaction kinetics and flow rates impact the length (L_{eq}) that particles travel on average before reaching chemical equilibrium with the mineral (Figures 7e and 7f). As flow rate increases, water particles travel longer paths on average before reaching chemical equilibrium. Regolith with a larger $\frac{C_{eq}}{R_{max}}$ also leads to a longer particle travel lengths on average before equilibrium is reached.

3.3.2 Temporal Characteristics of Weathering

Three factors affect the average time that it takes for particles to reach chemical equilibrium with the mineral (T_{eq}) (Figures 7a and 7b): (1) the exponential decline in K_s , with a smaller value of α parameter (less heterogeneous subsurface) resulting in equilibrium being reached faster; (2) the weathering reaction kinetics of the regolith with smaller $\frac{C_{eq}}{R_{max}}$ resulting in equilibrium being reached faster; and (3) flow rate, with an increase in flow rate the equilibrium is reached more rapidly. It is important to note that the calculated time to equilibrium (T_{eq}) is significantly higher than widely used mineral theoretical time to equilibrium which is assumed to be equal to $\frac{C_{eq}}{R_{max}}$ (shown for each mineral by dashed lines in Figures 7a and 7b). Albeit, for each mineral the calculated time to equilibrium begins to approach the theoretical one as the hillslope vertical heterogeneity in K_s pattern decreases and/or flow rate increases.

An increase in the rate of vertical decline in K_s increases the Damköhler number ($Da = \frac{MTT}{T_{eq}}$) (Figures 7c and 7d). This can be attributed to a larger increase in MTT (due to a longer old tale of TTD as shown in Figure 3) compared to T_{eq} (Figures 7a and 7b) as vertical heterogeneity in K_s increases. The mineral reaction kinetic also impacts the Damköhler number, with a smaller $\frac{C_{eq}}{R_{max}}$ resulting in a larger Damköhler number. An increase in flow rate also decreases the Damköhler number regardless of the regolith conductivity profile and mineral reaction kinetic. Note that based on the Damköhler number definition, as the Damköhler number

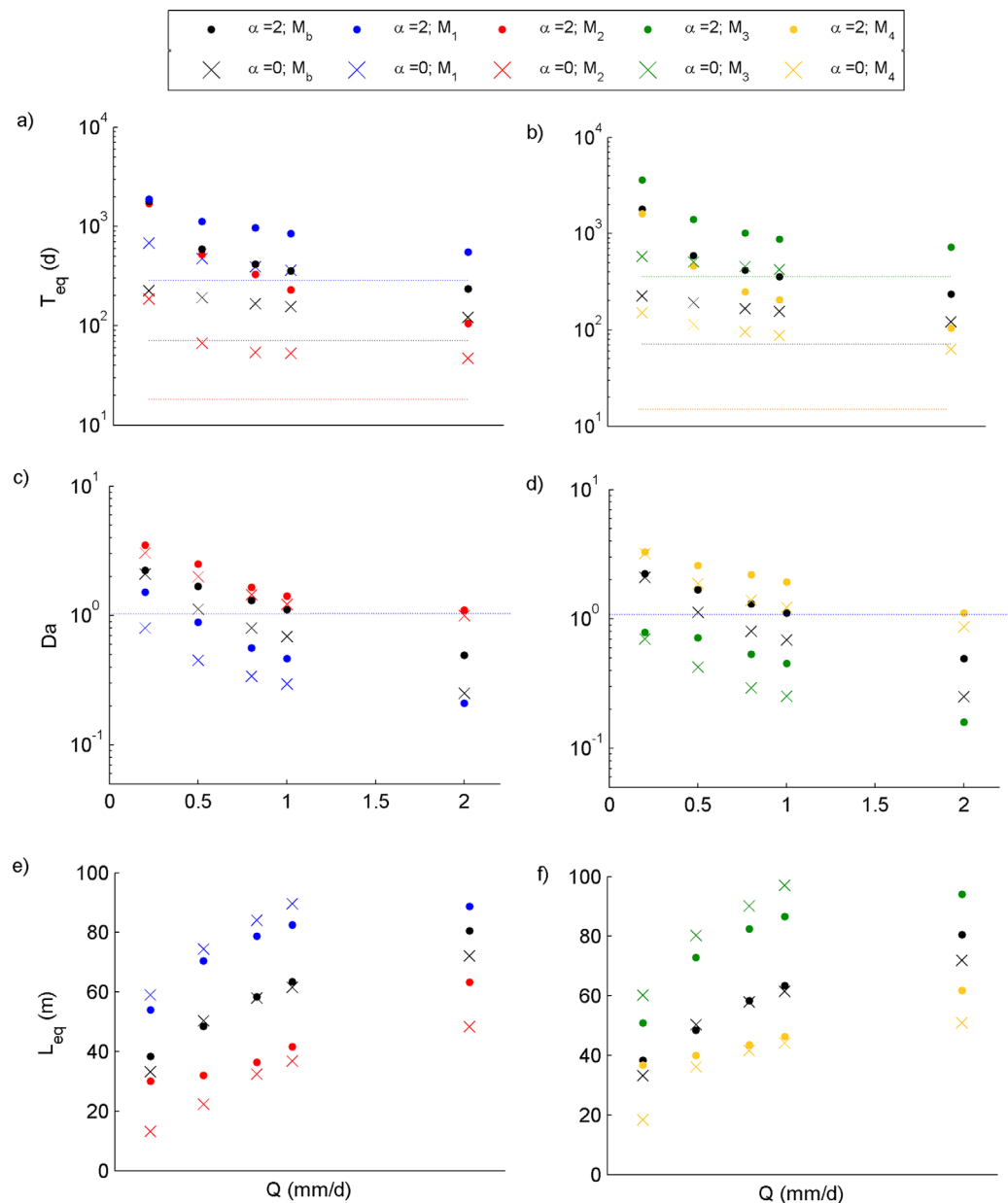


Figure 7. Hillslope average weathering characteristic versus flow rates for different exponential rates (α) of exponential decline in saturated hydraulic conductivity with soil depth and five theoretical minerals (M_b, M_1, M_2, M_3, M_4). Hillslope time to equilibrium (T_{eq}) for (a) minerals M_1, M_b , and M_2 where the mineral's $\frac{C_{sat}}{R_{max}}$ decreases among M_1, M_b , and M_2 and (b) minerals M_3, M_b , and M_4 where the mineral's $\frac{C_{sat}}{R_{max}}$ decreases among M_3, M_b , and M_4 . The dashed color (consistent with the mineral color) lines refer to the mineral theoretical time to equilibrium which is assumed to be equal to $\frac{C_{sat}}{R_{max}}$. The hillslope Damköhler number ($Da = \frac{MT}{T_{eq}}$) for (c) minerals M_1, M_b , and M_2 and (d) minerals M_3, M_b , and M_4 . Blue line refers to $Da = 1$ (the threshold between transport-controlled and surface reaction-controlled weathering regimes). Hillslope length to equilibrium (L_{eq}) for (e) minerals M_1, M_b , and M_2 and (f) minerals M_3, M_b , and M_4 . Within the homogeneous hillslope ($\alpha = 0$) and at high flow ($Q = 2$ mm/d), the chemical equilibrium condition is not reached for M_1 and M_3 minerals, and therefore the corresponding T_{eq}, L_{eq} , and Da number are not shown.

decreases, the regolith weathering regime approaches surface reaction-controlled (rather than transport-controlled) conditions.

3.3.3 Concentration-Residence Time Relations

Here we explore to what extent the water particle concentration within the hillslope can be related to the time (or residence time) that has elapsed since the particle entered the soil at the land surface (Figure 8). The Pearson correlation coefficient between concentration and residence time (ρ_{C-T}) throughout the hillslope becomes less strong as the rate of vertical exponential decline in K_s increases. The mineral with a

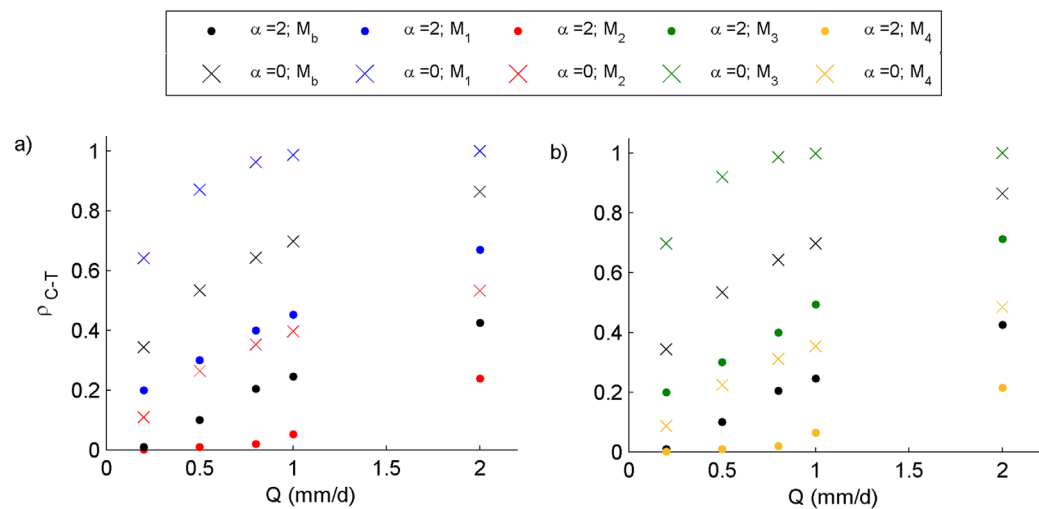


Figure 8. Pearson correlation coefficient between concentration and water residence time (ρ_{C-T}) for five minerals (M_b , M_1 , M_2 , M_3 , M_4), at streamflow rates varying from low flow to high flow and two saturated hydraulic conductivity vertical patterns ($\alpha = 0$ and $\alpha = 2$). Correlation coefficients for (a) minerals M_1 , M_b , and M_2 where the mineral's $\frac{C_{eq}}{R_{max}}$ decreases among M_1 , M_b , and M_2 and (b) minerals M_3 , M_b , and M_4 where the mineral's $\frac{C_{eq}}{R_{max}}$ decreases among M_3 , M_b , and M_4 . Residence time is the time which elapses between when a particle enters the soil at the land surface and when it reaches a given point within the hillslope. The calculated correlations are obtained from pairs of simulated concentration-residence time at 12,000 uniformly spaced points within the hillslope.

small $\frac{C_{eq}}{R_{max}}$ (e.g., M_2 and M_4) also shows lower ρ_{C-T} throughout the hillslope compared to the minerals with larger $\frac{C_{eq}}{R_{max}}$. These findings are further supported by the distribution of residence time and concentration throughout the hillslope shown in Figure 6. For both homogeneous and heterogeneous hillslopes, the spatial pattern of concentration becomes more similar to the spatial pattern of particle residence times (T_t) as $\frac{C_{eq}}{R_{max}}$ increases; albeit, this pattern is more pronounced for homogeneous hillslope compared to the heterogeneous one. The correlation between concentration and residence time within the hillslope is also enhanced with increasing the flow rate regardless of the regolith's conductivity profile and weathering reaction kinetics (Figure 8).

4. Discussion

Past studies have developed catchment-based chemical weathering models such as WITCH [Godd ris *et al.*, 2006], and soil profile chemical weathering models such as PROFILE [Sverdrup and Warfvinge, 1993]. All have sought to account for the processes controlling weathering characteristics, including ionic exchange, complexation with DOC, and precipitation of secondary phases. However, to date, representation of the subsurface vertical heterogeneity of the hydrological properties in the critical zone and their corresponding influence on flow pathlines and transit time distributions at different flow rates has not yet been examined in most current models of subsurface chemical weathering [Maher and Druhan, 2014].

Many investigations of weathering in the critical zone have focused on the unsaturated zone since gradients in water composition and mineral depletion are strongest in this zone, along with root uptake (there are some exceptions, such as Rempe and Dietrich [2014] and Anderson *et al.* [1997]). On the other hand, hydrologists that connect the catchment to stream discharge often focus on the saturated zone, as the unsaturated zone is often not an important source of stream discharge, particularly where steady or pseudo-steady flow conditions can be assumed. The simple hydrogeochemical model presented here (or the one offered by Maher and Druhan [2014]) provides an opportunity to build the dialogue between hydrologists and geochemists to advance the understanding of the feedbacks between hydrology and geochemistry in real-world catchments.

4.1. Simple Models to Explore Complex Behavior

This paper used a simplified catchment system to explore the interaction of flow pathlines, transit times and primary weathering characteristics together with the associated stream C-Q relations for weathering products. The starting point was an extension of the recently proposed integrated flow and transport

saturated-unsaturated model by Ameli *et al.* [2016a] to take weathering into account. This grid-free hydrological model has the ability to characterize time-invariant subsurface flow pathlines and transit time along these pathlines for subsurface flow rates and different degrees of exponential decline in saturated hydraulic conductivity (K_s) with depth. Recently, Ameli *et al.* [2016b] showed the importance of this decline in K_s for flow patterns and associated transit time distributions through catchments. Here we have coupled this semianalytical hydrological model with a general reversible TST-style rate law approach. This enables a theoretical exploration of the impact of the interaction between subsurface vertical heterogeneity in K_s , flow rate, and primary mineral weathering reaction kinetics on weathering evolution in the critical zone and the stream C-Q relations that this would produce. In reality, a host of other factors including pH, temperature, soil CO_2 pressure, DOC concentration, secondary mineral formation, and biological uptake will also affect chemical weathering evolution in the critical zone as well as the stream C-Q relation [Drever, 1994; Kim *et al.*, 2014; Oelkers, 2001; Oliva *et al.*, 1999; Sverdrup, 1990; White and Brantley, 1995]. However, the benefit of the proposed approach is the characterization of the interaction between subsurface hydrology and primary mineral reaction kinetic in a theoretical system, prior to considering other mechanisms in more complex models or in real systems.

4.1.1. Stream C-Q Relation

Vertical heterogeneity in hillslope conductivity is found to steepen the inverse relation between stream concentration and discharge. This is most accentuated for minerals with a large $\frac{C_{eq}}{R_{max}}$. As mineral R_{max} increases and/or C_{eq} decreases, vertical heterogeneity in K_s becomes a less important control, and the stream C-Q relation approaches chemostatic behavior. The mineral weathering reaction kinetic, flow rate, and K_s vertical heterogeneity also interact to change the average time (T_{eq}) and length (L_{eq}) at which chemical equilibrium is reached within the hillslope (Figure 7).

As flow rate increases, the weathering-derived concentration in young shallow waters that are discharged rapidly into the stream decreases. This leads to a stronger dilution of deeper high-concentration contributions by shallower low-concentration contributions as flow rates increase. An increase in R_{max} and/or decrease in C_{eq} (or in general decrease in $\frac{C_{eq}}{R_{max}}$) of mineral dissolution rate reduces the degree to which increased young water at high flow dilutes the concentration of the runoff water, since the concentration of the weathering product is almost identical in young and old waters (Figures 5a and 5b). This finding is important as recent global observations suggest that a large portion of global streamflow is less than 3 months old [Jasechko *et al.*, 2016]. Thus, as flow increases, diluted concentrations of weathering-derived products in streamflow may be expected in catchments with minerals that have a high ratio of $\frac{C_{eq}}{R_{max}}$ such as some silicate minerals (in circumneutral or at near-neutral pH) compared to the catchments with minerals that have a low ratio of $\frac{C_{eq}}{R_{max}}$ such as carbonate which typically shows chemostatic behavior.

4.1.2. Internal Weathering Regime Within the Hillslope

The developed model was able to explicitly calculate mean transit time (MTT) of water particles discharged into the stream as well as the average time (T_{eq}) at which chemical equilibrium is reached. Note that the former metric is often *implicitly* calculated using stream-rainfall tracer concentrations in hydrology [e.g., McGuire and McDonnell, 2006], and the latter is often assumed as equal to $\frac{C_{eq}}{R_{max}}$ in geochemistry [e.g., Maher and Chamberlain, 2014]. Damköhler numbers ($Da = \frac{MTT}{T_{eq}}$) thus could explicitly be calculated for each theoretical example presented here. Results suggest that vertical heterogeneity in K_s increases the Da . $Da < 1$ imply a surface reaction-controlled weathering condition within the hillslope, where fluid concentration is (on average) far enough from equilibrium with the mineral and mineral surfaces are available for further chemical weathering [Maher, 2010]. In contrast, $Da \geq 1$ suggests a transport-controlled weathering regime, where the fluid is (on average) approaching chemical equilibrium with the mineral, and only the removal of weathering products by aqueous transport can result in a departure from near thermodynamic equilibrium. But how are different weathering regimes in the hillslope linked to stream C-Q relations?

For theoretical mineral M_3 (the mineral with the largest $\frac{C_{eq}}{R_{max}}$), Da is much less than 1 for a range of flow rates, which implies a surface reaction-controlled weathering condition in the hillslope and leads to a strong inverse relation in the stream C-Q (compare Figures 4b and 7d). Indeed, as flow rate increases, the hillslope weathering condition moves from moderately ($Da < 1$) to strongly ($Da \ll 1$) surface reaction-controlled, which leads to a decrease in the concentration in the stream. Similarly, minerals M_1 and M_b with a large $\frac{C_{eq}}{R_{max}}$ of 285 d and moderate $\frac{C_{eq}}{R_{max}}$ of 71 d reveal strong (based on large best fit inverse power-law slope) inverse C-Q relation and moderate inverse C-Q relation, respectively; this can also be attributed to the hillslope internal weathering regimes with $Da < 1$ for a range of flow rates. On the other hand, for M_2 and M_4

(minerals with the smallest $\frac{C_{eq}}{R_{max}}$), Da numbers are close to 1 and larger for the range of flow rates considered. As flow rate increases, the weathering condition in the hillslope moves from more strongly transport-controlled ($Da \gg 1$) to moderately transport-controlled ($Da > 1$). This variation in hillslope internal weathering characteristic, however, results in only slight variation in stream concentration for a wide ranges of flow rate (compare Figures 4a and 4b and 7c and 7d). For M_2 and M_4 , an increase in flow rate can decrease MTT and thus the Da number, but it leads to only slight variation in the concentration in the stream as fluid is effectively always near equilibrium when discharged into the stream (i.e., small T_{eq} regardless of flow rate).

Exponential decline in K_s can enhance the concentration gradient within the hillslope for M_1 and M_3 (the minerals with the largest $\frac{C_{eq}}{R_{max}}$) (Figure 6). Further comparison between the spatial distribution of weathering product concentrations within the hillslope (Figure 6a) and the stream C-Q relation (Figures 4a and 4b) suggests that nonchemostatic stream concentration can result from stronger spatial heterogeneity in hillslope concentrations. Alternatively, chemostatic stream concentrations may result from a smaller concentration gradient within the hillslope. In the latter case, the subsurface conductivity profile (in terms of how K_s changes with depth) and the associated spatial and temporal patterns of water movement have small effects on the concentrations of weathering products within the hillslope and the subsequent stream C-Q relations. For this condition, simple displacement hydrogeochemical models might sufficiently predict stream C-Q relations [e.g., Robson *et al.*, 1992]. These findings are supported by large-scale measurements of concentration of weathering-derived products within the critical zone and stream performed by Herndon *et al.* [2015].

4.1.3. Theoretical Versus Calculated Time to Equilibrium

Explicit calculation of time to equilibrium (T_{eq}) suggests that T_{eq} is significantly larger than the theoretical time to equilibrium assumed to be equal to mineral $\frac{C_{eq}}{R_{max}}$. The latter has been widely used as a proxy for time to equilibrium in geochemistry [e.g., Maher and Chamberlain, 2014]. Time to equilibrium, however, begins to approach $\frac{C_{eq}}{R_{max}}$ as flow rate increases and/or vertical heterogeneity in hillslope conductivity decreases (Figures 7a and b). Our results also show that as $\frac{C_{eq}}{R_{max}}$ increases the stream C-Q varies from chemostatic to an inverse relation. Thus, theoretical time to equilibrium can be a useful measure for comparing stream C-Q relations across different landscapes. Furthermore, as mineral $\frac{C_{eq}}{R_{max}}$ decreases, the influence of the MTT on stream concentrations of weathering products decreases. This implies that MTT is not always a reliable predictor of stream concentrations of weathered-derived products.

4.2. Needs for Future Research

Our purely theoretical model demonstrated how the interaction between hillslope conductivity profile and mineral weathering reaction kinetics influence the spatial and temporal distribution of fluid concentrations in the saturated and unsaturated zones, as well as the stream C-Q relations of weathering products in the absence of other processes. Of course, the mineralogy in catchments is much more complex than in this demonstration, with a mixture of many fast-dissolving and slow-dissolving minerals, differing in the parameters n , R_{max} , and C_{eq} (see equation (3)). For example, in our demonstrations, mineral M_3 had the highest C_{eq} and took the longest time to reach its saturation state. If mineral M_2 , with the highest R_{max} , was also present, mineral M_3 would have reached equilibrium much faster. In addition, while C_{eq} is an inherent property of the mineral, the R_{max} can be viewed as the product between the specific dissolution rate and the reactive surface area; commonly, the more reactive minerals are also less abundant, because they have simply dissolved during soil development. The dissolution of one mineral may then affect the dissolution of others, as a fast-dissolving mineral will release more weathering products that inhibit the dissolution of slow-weathering minerals. Different ions can also display different stream C-Q relations for the same sites [Ledesma *et al.*, 2013], which may be a consequence of the fact that Na^+ -bearing and K^+ -bearing minerals tend to dissolve more slowly than Ca^{2+} -bearing and Mg^{2+} -bearing minerals [Sverdrup, 1990]. Lateral variations in saturated hydraulic conductivity, local scale heterogeneities in chemical characteristics in different parts of the pore space may also complicate the actual distribution of weathering rates and weathering product concentrations in space and time [e.g., Neal *et al.*, 1992; Stonestrom *et al.*, 1998].

Here we have chosen an idealized representation of the hillslope, where the dissolution rate at far-from-equilibrium conditions is represented by a plateau. In reality, there are other factors controlling mineral dissolution rates aside from the chemical affinity (i.e., distance to equilibrium). The most influential factors in a hillslope are likely to be the reactive surface area and pH. The surface area of reactive minerals tends to decrease with depth, which will cause the net dissolution rates to decrease. pH tends to increase with

increasing water transit time, which will cause a decrease in dissolution rates for most minerals. Thus, net dissolution rates would probably not be constant with increasing transit time, but instead display a gently decreasing slope. However, for the purpose of illustrating how mineral dissolution kinetics can influence in-stream patterns of water chemistry, these simplifications are justified. A natural next step would be to go from theoretical demonstrations to using real data and more complex 3-D models that seek to account for more of the fundamental processes [cf. *Ibarra et al.*, 2016]. This would involve testing models against observed stream C-Q relations of weathering-derived elements in the critical zone and streams. It would also involve using the observed mineralogy together with dissolution rate laws based on empirical observations and associated processes under more realistic modeling assumptions.

Of course, future modeling-observation experiments require dynamic integrated flow and weathering transport models to take into account the association between time-variant transit times [e.g., *Botter*, 2012; *Harman*, 2015; *Heidbüchel et al.*, 2013; *Kirchner*, 2016b; *Velde et al.*, 2012] and transient stream concentrations as the hillslopes wets and dries. *Anderson et al.* [1997] as well as other classic field studies [e.g., *Miller and Drever*, 1977; *Walling and Foster*, 1975] clearly demonstrated a transient increase in weathering-derived stream concentration at the beginning of a flow event (i.e., during the rising limb of the stream hydrograph). *Neal and Kirchner* [2000] and *Kirchner et al.* [2000] also depicted the presence of a strong transiency in the stream concentration of weathering-derived constituents within the Plynlimon catchment based on daily to weekly stream chemistry measurements. The steady state condition, however, is still a necessary assumption for most chemical weathering models, including the one used in this paper. While these kind of models may still be valid for the simulation of reactive solute transport farther away from the soil surface [e.g., *Destouni*, 1991] and for the simulation of long-term chemical behavior of catchments with little seasonality [e.g., *Botter et al.*, 2010], simulation of short-term storm dynamics on stream concentration will require a model with the ability to take into account the mixing and displacement of both fast flow pathways and stored old waters at event timescales. This can be accomplished through coupling an appropriate dissolution rate law approach with fully dynamic integrated subsurface flow and particle movement approaches such as MIPS [*Davies et al.*, 2011, 2013] or a transient version of the present semianalytical solution.

Lastly, our intention with this paper was to identify the controls created by the primary weathering of minerals as one component of the complete “picture.” It is unclear whether there actually exists any true equilibrium for dissolution of primary minerals in catchments as the dissolution of most primary minerals is an irreversible process at low temperatures [*Sverdrup*, 1990]. However, it is undisputed that mineral dissolution is significantly inhibited by high concentrations of weathering products (which is captured by the simple model used in this study, although the exact shape of the dissolution rate-function dependence near equilibrium is not known). Furthermore, it is clear that the relation between subsurface conductivity profile, transit time, and the primary weathering characteristics gives rise to distinct stream C-Q-relations.

5. Conclusion

We coupled a novel integrated saturated-unsaturated flow and particle tracking transport model with the Transition State Theory style dissolution rate law approach to theoretically explore the impact of the interaction between vertical heterogeneity in saturated hydraulic conductivity (K_s), mineral weathering reaction kinetics, and flow rate on chemical weathering evolution in the critical zone and stream concentration-discharge relations. Subsurface vertical heterogeneity in K_s pattern augments heterogeneity in the distribution of fluid concentration in the critical zone as well as contributes to an inverse clockwise C-Q relation in the stream. However, as the ratio of mineral equilibrium concentration to intrinsic weathering rate ($\frac{C_{eq}}{R_{max}}$) decreases, the stream C-Q relation approaches an approximate chemostatic behavior, regardless of the degree of subsurface vertical heterogeneity in the K_s pattern. The vertical heterogeneity in K_s pattern also affects chemical equilibrium time and length, but this effect declines as the mineral $\frac{C_{eq}}{R_{max}}$ decreases. Stream concentration also becomes less dependent on time-invariant mean transit time again as the mineral $\frac{C_{eq}}{R_{max}}$ decreases.

Our findings, despite the simplifications employed, can help to improve the understanding of the potential consequences of future climatic and land use variations on hillslope and stream concentrations of

weathering-derived products in catchments with different substrate heterogeneity. Future research will be needed to couple the current theoretical approach with realistic subsurface mineralogy as well as detailed concentrations of weathered-derived products in streams. Such integration will help to answer questions about the validity and applicability of dissolution rate law approaches under different hydrological and subsurface conductivity profile scenarios.

Appendix A: Semianalytical Series Solution for Saturated-Unsaturated Flow

Ameli et al. [2016a] have shown that the series solution to the *unsaturated* flow governing equation with no-flow conditions along the sides of the unsaturated domain and exponentially depth decaying saturated hydraulic conductivity with soil depth ($K_s = K_{s0} e^{\alpha(z-z_t)}$) can be calculated in terms of Kirchhoff potential (ϕ_u) as

$$\phi_u(x, z) = A_0 [\exp(-\beta z)] - \sum_{m=1}^M \left(A_m \left[\cos\left(\frac{m\pi}{L}x\right) \exp(\xi_m z) \right]^{\frac{\xi_m}{L}} + B_m \left[\cos\left(\frac{m\pi}{L}x\right) \exp(\bar{\xi}_m z) \right]^{\frac{\bar{\xi}_m}{L}} \right) \tag{A1}$$

$$\xi_m = \frac{-(\alpha + \beta)}{2} + \frac{1}{2} \sqrt{(\alpha + \beta)^2 - 4\alpha\beta + \left(\frac{2m\pi}{L}\right)^2}, \quad \bar{\xi}_m = \frac{-(\alpha + \beta)}{2} - \frac{1}{2} \sqrt{(\alpha + \beta)^2 - 4\alpha\beta + \left(\frac{2m\pi}{L}\right)^2}$$

where $\phi_u(\varphi) = \frac{K_{s0} \exp(\beta(\varphi - \varphi^e))}{\beta}$

The series solution for the *saturated* moisture movement with exponentially depth decaying saturated hydraulic conductivity with soil depth ($K_s = K_{s0} e^{\alpha(z-z_t)}$) can also be calculated in terms of discharge potential function ($\phi_s(x, z)$) as

$$\phi_s(x, z) = C_0 + \sum_{n=1}^N \left(C_n \left[\cos\left(\frac{n\pi}{L}x\right) \exp(\gamma_n z) \right] + D_n \left[\cos\left(\frac{n\pi}{L}x\right) \exp(\bar{\gamma}_n z) \right] \right) \tag{A2}$$

$$\gamma_n = \frac{-\alpha}{2} + \frac{1}{2} \sqrt{\alpha^2 + \left(\frac{2n\pi}{L}\right)^2}, \quad \bar{\gamma}_n = \frac{-\alpha}{2} - \frac{1}{2} \sqrt{\alpha^2 + \left(\frac{2n\pi}{L}\right)^2}$$

where $\phi_s(x, z) = K_{s0} h_s(x, z)$

In equations (A1) and (A2), h_s [L] refers to the total hydraulic head, $\varphi(x, z)$ represents suction pressure head [L], L is aquifer length, K_{s0} [LT^{-1}] refers to the saturated hydraulic conductivity along the topographic surface ($z_t(x)$), α is the parameter of the exponential relationship between saturated hydraulic conductivity with soil depth, β and φ^e denote the sorptive numbers of the Gardner’s constitutive function [Gardner, 1958] used in this paper to characterize the φ - K_s relationship in the unsaturated zone. In the above equations, additionally, m and n are the coefficient index, and A_0 , A_m , B_m , C_0 , C_n , and D_n refer to the unknown series coefficients associated with the m th and n th coefficient indices, respectively. In addition, M and N are the total number of terms in the series solutions to the unsaturated and saturated flow governing equations, respectively. The unknown series solution coefficients (A_0 , A_m , B_m , C_0 , C_n , D_n) for equations (A1) and (A2) were calculated by enforcing the boundary conditions at the top and the bottom of saturated and unsaturated zones using a least square scheme. The a priori unknown location of water table was also calculated using a robust iterative scheme. We refer the readers to Ameli et al. [2016a] for a detailed discussion of the mathematical formulation of saturated and unsaturated governing equations, series solution method, boundary conditions, least square scheme used to enforce boundary conditions, and iterative algorithm used to determine the a priori unknown location of water table.

The calculated Kirchhoff potential function (equation (A1)) and discharge potential function (equation (A2)) in the unsaturated and saturated zones, respectively, can be used to determine continuous maps of Darcy-Buckingham fluxes in the unsaturated zone ($q_{ux}(x, z)$ and $q_{uz}(x, z)$), and Darcy fluxes throughout the entire saturated zone ($q_{sx}(x, z)$ and $q_{sz}(x, z)$) as

$$q_{ux}(x, z) = e^{\alpha(z-z_t)} \frac{d\phi_u(x, z)}{dx} \quad \text{and} \quad q_{uz}(x, z) = e^{\alpha(z-z_t)} \left(\frac{d\phi_u(x, z)}{dz} + \beta \phi_u(x, z) \right) \tag{A3}$$

$$q_{sx}(x, z) = e^{\alpha(z-z_t)} \frac{d\phi_s(x, z)}{dx} \quad \text{and} \quad q_{sz}(x, z) = e^{\alpha(z-z_t)} \frac{d\phi_s(x, z)}{dz} \quad (\text{A4})$$

Continuous fields of pore water velocity in the unsaturated and saturated zones and in both x and y directions are then calculated as

$$V_{ux}(x, z) = \frac{q_{ux}(x, z)}{\theta_u(x, z)} \quad \text{and} \quad V_{uz}(x, z) = \frac{q_{uz}(x, z)}{\theta_u(x, z)} \quad (\text{A5})$$

$$V_{sx}(x, z) = \frac{q_{sx}(x, z)}{\theta_s(x, z)} \quad \text{and} \quad V_{sz}(x, z) = \frac{q_{sz}(x, z)}{\theta_s(x, z)} \quad (\text{A6})$$

In equations (A5) and (A6), the unsaturated moisture content (θ_u) is obtained based on both the suction pressure head (φ) and soil depth at each location ($\theta_u(x, z, \varphi) = \theta_{s0}(x, z) e^{\alpha(z-z_t)} e^{\beta(\varphi - \varphi^e)}$). In addition, the saturated moisture content (θ_s) is assumed to be equal to the porosity and is obtained as a function of soil depth $\theta_s(x, z) = \theta_{s0}(x, z) e^{\alpha(z-z_t)}$.

Acknowledgments

We thank three anonymous reviewers of the Water Resources Research journal for their constructive comments. This research was funded by NSERC Discovery Grant and NSERC Accelerator to J.J.M., NSERC Discovery Grant to I.F.C. The Krycklan catchment study is supported by the Swedish Science Foundation (VR) SITES, ForWater (Formas), Future Forest, Kempe Foundation, SLU FOMA, and SKB. The data used for all simulations are available upon request from the corresponding author.

References

- Ameli, A. A., J. Craig, and J. McDonnell (2015), Are all runoff processes the same? Numerical experiments comparing a Darcy-Richards solver to an overland flow-based approach for subsurface storm runoff simulation, *Water Resour. Res.*, *51*, 10,008–10,028, doi:10.1002/2015WR017199.
- Ameli, A. A., J. J. McDonnell, and K. Bishop (2016a), The exponential decline in saturated hydraulic conductivity with depth and its effect on water flow paths and transit time distribution, *Hydrol. Processes*, *30*(14), 12.
- Ameli, A. A., N. Amvrosiadi, T. Grabs, H. Laudon, I. Creed, J. McDonnell, and K. Bishop (2016b), Hillslope permeability architecture controls on subsurface transit time distribution and flow paths, *J. Hydrol.*, *543*, 17–30.
- Anderson, S. P., and W. E. Dietrich (2001), Chemical weathering and runoff chemistry in a steep headwater catchment, *Hydrol. Processes*, *15*(10), 1791–1815.
- Anderson, S. P., W. E. Dietrich, R. Torres, D. R. Montgomery, and K. Loague (1997), Concentration-discharge relationships in runoff from a steep, unchanneled catchment, *Water Resour. Res.*, *33*(1), 211–225.
- Atchley, A. L., A. K. Navarre-Sitchler, and R. M. Maxwell (2014), The effects of physical and geochemical heterogeneities on hydro-geochemical transport and effective reaction rates, *J. Contam. Hydrol.*, *165*, 53–64.
- Bishop, K., J. Seibert, S. Köhler, and H. Laudon (2004), Resolving the Double Paradox of rapidly mobilized old water with highly variable responses in runoff chemistry, *Hydrol. Processes*, *18*(1), 185–189.
- Bishop, K., J. Seibert, L. Nyberg, and A. Rodhe (2011), Water storage in a till catchment. II: Implications of transmissivity feedback for flow paths and turnover times, *Hydrol. Processes*, *25*(25), 3950–3959.
- Botter, G. (2012), Catchment mixing processes and travel time distributions, *Water Resour. Res.*, *48*, W05545, doi:10.1029/2011WR011160.
- Botter, G., E. Bertuzzo, and A. Rinaldo (2010), Transport in the hydrologic response: Travel time distributions, soil moisture dynamics, and the old water paradox, *Water Resour. Res.*, *46*, W03514, doi:10.1029/2009WR008371.
- Brantley, S., J. Megonigal, F. Scatena, Z. Balogh-Brunstad, R. Barnes, M. Bruns, P. Van Cappellen, K. Dontsova, H. Hartnett, and A. Hartshorn (2011), Twelve testable hypotheses on the geobiology of weathering, *Geobiology*, *9*(2), 140–165.
- Burns, D. A., R. P. Hooper, J. J. McDonnell, J. E. Freer, C. Kendall, and K. Beven (1998), Base cation concentrations in subsurface flow from a forested hillslope: The role of flushing frequency, *Water Resour. Res.*, *34*(12), 3535–3544.
- Burns, D. A., L. N. Plummer, J. J. McDonnell, E. Busenberg, G. C. Casile, C. Kendall, R. P. Hooper, J. E. Freer, N. E. Peters, and K. Beven (2003), The geochemical evolution of riparian ground water in a forested piedmont catchment, *Groundwater*, *41*(7), 913–925.
- Chanat, J. G., K. C. Rice, and G. M. Hornberger (2002), Consistency of patterns in concentration-discharge plots, *Water Resour. Res.*, *38*(8), doi:10.1029/2001WR000971.
- Clow, D., and J. Drever (1996), Weathering rates as a function of flow through an alpine soil, *Chem. Geol.*, *132*(1), 131–141.
- Cui, Z., C. Welty, and R. M. Maxwell (2014), Modeling nitrogen transport and transformation in aquifers using a particle-tracking approach, *Comput. Geosci.*, *70*, 1–14.
- Davies, J., K. Beven, L. Nyberg, and A. Rodhe (2011), A discrete particle representation of hillslope hydrology: Hypothesis testing in reproducing a tracer experiment at Gårdsjön, Sweden, *Hydrol. Processes*, *25*(23), 3602–3612.
- Davies, J., K. Beven, A. Rodhe, L. Nyberg, and K. Bishop (2013), Integrated modeling of flow and residence times at the catchment scale with multiple interacting pathways, *Water Resour. Res.*, *49*, 4738–4750, doi:10.1002/wrcr.20377.
- Davies, J. A., and K. Beven (2015), Hysteresis and scale in catchment storage, flow and transport, *Hydrol. Processes*, *29*(16), 3604–3615.
- Destouni, G. (1991), Applicability of the steady state flow assumption for solute advection in field soils, *Water Resour. Res.*, *27*(8), 2129–2140.
- Drever, J., and L. Stillings (1997), The role of organic acids in mineral weathering, *Colloids Surf. A*, *120*(1), 167–181.
- Drever, J. I. (1988), *The Geochemistry of Natural Waters*, Prentice Hall, Englewood Cliffs, N. J.
- Drever, J. I. (1994), The effect of land plants on weathering rates of silicate minerals, *Geochim. Cosmochim. Acta*, *58*(10), 2325–2332.
- Erlandsson, M., E. Oelkers, K. Bishop, H. Sverdrup, S. Belyazid, J. Ledesma, and S. Köhler (2016), Spatial and temporal variations of base cation release from chemical weathering on a hillslope scale, *Chem. Geol.*, *441*, 1–13.
- Evans, C., and T. D. Davies (1998), Causes of concentration/discharge hysteresis and its potential as a tool for analysis of episode hydro-chemistry, *Water Resour. Res.*, *34*(1), 129–137.
- Eyring, H. (1935), The activated complex in chemical reactions, *J. Chem. Phys.*, *3*(2), 107–115.
- Gaillardet, J., S. Rad, K. Rivié, P. Louvat, C. Gorge, C. J. Allègre, and E. Lajeunesse (2011), Orography-driven chemical denudation in the Lesser Antilles: Evidence for a new feed-back mechanism stabilizing atmospheric CO₂, *Am. J. Sci.*, *311*(10), 851–894.
- Gardner, W. (1958), Some steady-state solutions of the unsaturated moisture flow equation with application to evaporation from a water table, *Soil Sci.*, *85*(4), 228–232.

- Goddéris, Y., L. M. François, A. Probst, J. Schott, D. Moncoulon, D. Labat, and D. Viville (2006), Modelling weathering processes at the catchment scale: The WITCH numerical model, *Geochim. Cosmochim. Acta*, *70*(5), 1128–1147.
- Godsey, S. E., J. W. Kirchner, and D. W. Clow (2009), Concentration-discharge relationships reflect chemostatic characteristics of US catchments, *Hydrol. Processes*, *23*(13), 1844–1864.
- Golubev, S. V., O. S. Pokrovsky, and J. Schott (2005), Experimental determination of the effect of dissolved CO₂ on the dissolution kinetics of Mg and Ca silicates at 25 C, *Chem. Geol.*, *217*(3), 227–238.
- Harman, C. J. (2015), Time-variable transit time distributions and transport: Theory and application to storage-dependent transport of chloride in a watershed, *Water Resour. Res.*, *51*, 1–30, doi:10.1002/2014WR015707.
- Heidbüchel, I., P. A. Troch, and S. W. Lyon (2013), Separating physical and meteorological controls of variable transit times in zero-order catchments, *Water Resour. Res.*, *49*, 7644–7657, doi:10.1002/2012WR013149.
- Hellmann, R. (1994), The albite-water system: Part I. The kinetics of dissolution as a function of pH at 100, 200 and 300°C, *Geochim. Cosmochim. Acta*, *58*(2), 595–611.
- Hem, J. D. (1948), Fluctuations in concentration of dissolved solids of some southwestern streams, *Eos Trans. AGU*, *29*(1), 80–84.
- Herndon, E. M., A. L. Dere, P. L. Sullivan, D. Norris, B. Reynolds, and S. L. Brantley (2015), Landscape heterogeneity drives contrasting concentration-discharge relationships in shale headwater catchments, *Hydrol. Earth Syst. Sci.*, *19*, 3333.
- Ibarra, D. E., J. K. Caves, S. Moon, D. L. Thomas, J. Hartmann, C. P. Chamberlain, and K. Maher (2016), Differential weathering of basaltic and granitic catchments from concentration-discharge relationships, *Geochim. Cosmochim. Acta*, *190*, 265–293.
- Jasechko, S., J. W. Kirchner, J. M. Welker, and J. J. McDonnell (2016), Substantial proportion of global streamflow less than three months old, *Nat. Geosci.*, *9*, 126–129.
- Johnson, N. M., G. E. Likens, F. Bormann, D. Fisher, and R. Pierce (1969), A working model for the variation in stream water chemistry at the Hubbard Brook Experimental Forest, New Hampshire, *Water Resour. Res.*, *5*(6), 1353–1363.
- Johnson, T. M., and D. J. DePaolo (1994), Interpretation of isotopic data in groundwater-rock systems: Model development and application to Sr isotope data from Yucca Mountain, *Water Resour. Res.*, *30*(5), 1571–1587.
- Kim, H., J. K. Bishop, W. E. Dietrich, and I. Y. Fung (2014), Process dominance shift in solute chemistry as revealed by long-term high-frequency water chemistry observations of groundwater flowing through weathered argillite underlying a steep forested hillslope, *Geochim. Cosmochim. Acta*, *140*, 1–19.
- Kirchner, J. (2016a), Aggregation in environmental systems—Part 1: Seasonal tracer cycles quantify young water fractions, but not mean transit times, in spatially heterogeneous catchments, *Hydrol. Earth Syst. Sci.*, *20*, 279–297.
- Kirchner, J. (2016b), Aggregation in environmental systems—Part 2: Catchment mean transit times and young water fractions under hydrologic nonstationarity, *Hydrol. Earth Syst. Sci.*, *20*, 299–328.
- Kirchner, J. W., X. Feng, and C. Neal (2000), Fractal stream chemistry and its implications for contaminant transport in catchments, *Nature*, *403*(6769), 524–527.
- Lasaga, A. C. (2014), *Kinetic Theory in the Earth Sciences*, Princeton Univ. Press.
- Lasaga, A. C., and R. J. Kirkpatrick (1981), *Kinetics of Geochemical Processes*, *Rev. Mineral.*, vol. 8, Mineral. Soc. of Am., Washington, D. C.
- Lebedeva, M., R. Fletcher, V. Balashov, and S. Brantley (2007), A reactive diffusion model describing transformation of bedrock to saprolite, *Chem. Geol.*, *244*(3), 624–645.
- Ledesma, J., T. Grabs, M. Futter, K. H. Bishop, H. Laudon, and S. Köhler (2013), Riparian zone control on base cation concentration in boreal streams, *Biogeosciences*, *10*(6), 3849–3868.
- Maher, K. (2010), The dependence of chemical weathering rates on fluid residence time, *Earth Planet. Sci. Lett.*, *294*(1), 101–110.
- Maher, K. (2011), The role of fluid residence time and topographic scales in determining chemical fluxes from landscapes, *Earth Planet. Sci. Lett.*, *312*(1), 48–58.
- Maher, K., and C. Chamberlain (2014), Hydrologic regulation of chemical weathering and the geologic carbon cycle, *Science*, *343*(6178), 1502–1504.
- Maher, K., and J. Druhan (2014), Relationships between the transit time of water and the fluxes of weathered elements through the critical zone, *Proc. Earth Planet. Sci.*, *10*, 16–22.
- Maher, K., C. I. Steefel, A. F. White, and D. A. Stonestrom (2009), The role of reaction affinity and secondary minerals in regulating chemical weathering rates at the Santa Cruz Soil Chronosequence, California, *Geochim. Cosmochim. Acta*, *73*(10), 2804–2831.
- Manning, A. H., P. L. Verplanck, J. S. Caine, and A. S. Todd (2013), Links between climate change, water-table depth, and water chemistry in a mineralized mountain watershed, *Appl. Geochem.*, *37*, 64–78.
- McDonnell, J. J., and K. Beven (2014), Debates—The future of hydrological sciences: A (common) path forward? A call to action aimed at understanding velocities, celerities and residence time distributions of the headwater hydrograph, *Water Resour. Res.*, *50*, 5342–5350, doi:10.1002/2013WR015141.
- McGlynn, B. L., and J. J. McDonnell (2003), Role of discrete landscape units in controlling catchment dissolved organic carbon dynamics, *Water Resour. Res.*, *39*(4), 1090, doi:10.1029/2002WR001525.
- McGuire, K. J., and J. J. McDonnell (2006), A review and evaluation of catchment transit time modeling, *J. Hydrol.*, *330*(3), 543–563.
- Miller, W. R., and J. I. Drever (1977), Water chemistry of a stream following a storm, Absaroka Mountains, Wyoming, *Geol. Soc. Am. Bull.*, *88*(2), 286–290.
- Moon, S., C. Chamberlain, and G. Hilley (2014), New estimates of silicate weathering rates and their uncertainties in global rivers, *Geochim. Cosmochim. Acta*, *134*, 257–274.
- Neal, C., and J. W. Kirchner (2000), Sodium and chloride levels in rainfall, mist, streamwater and groundwater at the Plynlimon catchments, mid-Wales: Inferences on hydrological and chemical controls, *Hydrol. Earth Syst. Sci. Discuss.*, *4*(2), 295–310.
- Neal, C., B. Reynolds, C. Smith, S. Hill, M. Neal, T. Conway, G. Ryland, H. Jeffrey, A. Robson, and R. Fisher (1992), The impact of conifer harvesting on stream water pH, alkalinity and aluminium concentrations for the British uplands: An example for an acidic and acid sensitive catchment in mid-Wales, *Sci. Total Environ.*, *126*(1–2), 75–87.
- Oelkers, E. H. (2001), General kinetic description of multioxide silicate mineral and glass dissolution, *Geochim. Cosmochim. Acta*, *65*(21), 3703–3719.
- Oelkers, E. H., and J. Schott (2001), An experimental study of enstatite dissolution rates as a function of pH, temperature, and aqueous Mg and Si concentration, and the mechanism of pyroxene/pyroxenoid dissolution, *Geochim. Cosmochim. Acta*, *65*(8), 1219–1231.
- Oelkers, E. H., J. Schott, and J.-L. Devidal (1994), The effect of aluminum, pH, and chemical affinity on the rates of aluminosilicate dissolution reactions, *Geochim. Cosmochim. Acta*, *58*(9), 2011–2024.
- Oliva, P., J. Viers, B. Dupré, J. P. Fortuné, F. Martin, J. J. Braun, D. Nahon, and H. Robain (1999), The effect of organic matter on chemical weathering: Study of a small tropical watershed: Nsimi-Zoetele site, Cameroon, *Geochim. Cosmochim. Acta*, *63*(23), 4013–4035.

- Palandri, J. L., and Y. K. Kharaka (2004), A compilation of rate parameters of water-mineral interaction kinetics for application to geochemical modeling, DTIC Document, *U.S. Geol. Surv. Open File Rep.*, 2004-1068.
- Pilgrim, D. H., D. D. Huff, and T. D. Steele (1979), Use of specific conductance and contact time relations for separating flow components in storm runoff, *Water Resour. Res.*, 15(2), 329–339.
- Rempe, D. M., and W. E. Dietrich (2014), A bottom-up control on fresh-bedrock topography under landscapes, *Proc. Natl. Acad. Sci. U. S. A.*, 111(18), 6576–6581.
- Robson, A., K. Beven, and C. Neal (1992), Towards identifying sources of subsurface flow: A comparison of components identified by a physically based runoff model and those determined by chemical mixing techniques, *Hydrol. Processes*, 6(2), 199–214.
- Siirila, E. R., and R. M. Maxwell (2012), Evaluating effective reaction rates of kinetically driven solutes in large-scale, statistically anisotropic media: Human health risk implications, *Water Resour. Res.*, 48, W04527, doi:10.1029/2011WR011516.
- Stonestrom, D. A., A. F. White, and K. C. Akstin (1998), Determining rates of chemical weathering in soils—Solute transport versus profile evolution, *J. Hydrol.*, 209(1), 331–345.
- Sverdrup, H., and P. Warfvinge (1993), Calculating field weathering rates using a mechanistic geochemical model PROFILE, *Appl. Geochem.*, 8(3), 273–283.
- Sverdrup, H. U. (1990), *The Kinetics of Base Cation Release Due to Chemical Weathering*, 245 pp., Lund Univ. Press, Lund, Sweden.
- Torres, M. A., A. J. West, and K. E. Clark (2015), Geomorphic regime modulates hydrologic control of chemical weathering in the Andes–Amazon, *Geochim. Cosmochim. Acta*, 166, 105–128.
- Velde, v. d. Y., P. Torfs, S. Zee, and R. Uijlenhoet (2012), Quantifying catchment-scale mixing and its effect on time-varying travel time distributions, *Water Resour. Res.*, 48, W06536, doi:10.1029/2011WR011310.
- Walling, D., and I. Foster (1975), Variations in the natural chemical concentration of river water during flood flows, and the lag effect: Some further comments, *J. Hydrol.*, 26(3–4), 237–244.
- White, A. F., and S. L. Brantley (1995), Chemical weathering rates of silicate minerals: An overview, *Chem. Weathering Rates Silicate Minerals*, 31, 1–22.
- White, A. F., M. S. Schulz, D. V. Vivit, A. E. Blum, D. A. Stonestrom, and S. P. Anderson (2008), Chemical weathering of a marine terrace chronosequence, Santa Cruz, California I: Interpreting rates and controls based on soil concentration-depth profiles, *Geochim. Cosmochim. Acta*, 72(1), 36–68.
- White, A. F., M. S. Schulz, D. A. Stonestrom, D. V. Vivit, J. Fitzpatrick, T. D. Bullen, K. Maher, and A. E. Blum (2009), Chemical weathering of a marine terrace chronosequence, Santa Cruz, California. Part II: Solute profiles, gradients and the comparisons of contemporary and long-term weathering rates, *Geochim. Cosmochim. Acta*, 73(10), 2769–2803.
- Zakharova, E., O. Pokrovsky, B. Dupré, and M. Zaslavskaya (2005), Chemical weathering of silicate rocks in Aldan Shield and Baikal Uplift: Insights from long-term seasonal measurements of solute fluxes in rivers, *Chem. Geol.*, 214(3), 223–248.
- Zhu, C. (2005), In situ feldspar dissolution rates in an aquifer, *Geochim. Cosmochim. Acta*, 69(6), 1435–1453.